Modeling the IntraCluster Medium

Michael Peel

Literature Review

Supervisors: Ian Browne & Richard Battye

Department of Physics and Astronomy
The University of Manchester

15 December 2006

Abstract

Observations of clusters of galaxies present a unique probe of cosmological parameters. We summarize the observations that can be made of the cluster galaxies and the IntraCluster Medium, and examine the measurements of cosmological parameters that can subsequently be obtained. We then discuss at the common components of analytical models of the IntraCluster Medium, and review three models. Finally, we look at the types of numerical simulations that can be utilized to simulate clusters of galaxies, including various N-body and hydrodynamic schemes.

1 Introduction

The IntraCluster Medium (ICM), also known as the intergalactic medium or the intracluster plasma, consists of a dark matter halo and a hot baryonic gas located at the centre of clusters of galaxies. The gas is heated predominantly by energy from the cluster's gravitational well, although other effects also provide a source of energy. Due to its temperature, it emits in X-rays thermally, and it can also be observed via its effect on photons from the Cosmic Microwave Background (CMB). It has cosmological importance as it provides a tracer for locating clusters of galaxies, the distribution of which can provide constraints on fundamental cosmological parameters.

In general, a cluster is defined as a set of over 50 galaxies in close ($\lesssim$ 2Mpc) proximity to each other, following the pioneering work done by Abell (1958). Sets of galaxies smaller than this are termed "galaxy groups". In addition, clusters of galaxies can be allotted a "richness" depending on the number of galaxies within them (see Table 2).

Only about 10% of the baryonic mass of clusters is in the galaxies in the cluster; the remainder is in the intracluster medium. In turn, the baryonic mass is only around a seventh of the total mass of the cluster (Ostriker et al., 2005). As such, individual galaxies are generally neglected in models of the intracluster medium, although some effects that result from the galaxies may need to be accounted for.

§2 of this review discusses the various ways by which clusters can be observed, and what can be seen by each observational method. §3 discusses the cosmological effects and results of clusters. §4 covers several approaches to analytical models of the intracluster medium, while §5 reviews the various types of computational simulations that can be utilized. §6 concludes the report.

Further information along a similar vein as this article can be found in the review by Voit (2004).

2 Observations

Observations of clusters of galaxies utilize a wide variety of frequencies. Optical and infrared observations locate individual galaxies, while observations through X-rays and microwaves can detect the intracluster medium.

Richness class	Galaxy counts
0	30–49
1	50–79
2	80–129
3	130–199
4	200–299
5	300 or over

Table 1: Richness classes, as defined by Abell (1958).

2.1 Optical and infrared

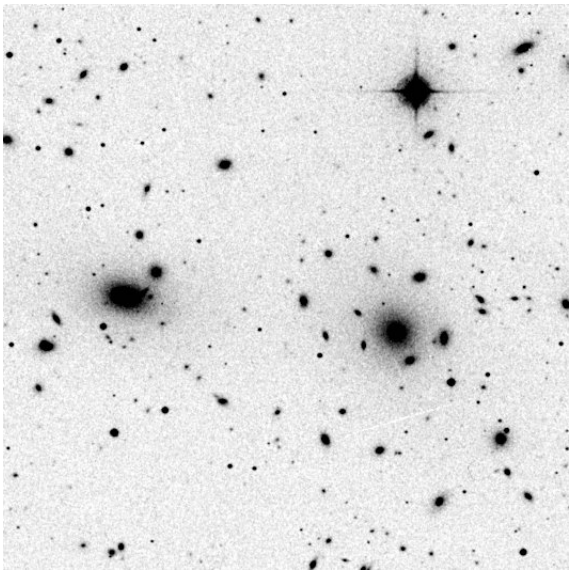

Figure 1: The Coma Cluster (Abell 1656) at 645nm. From the *Digitized Sky Survey*.

Clusters of galaxies have been identified using optical wavelengths since the late 18^{th} century (see Biviano, 2000, for a historical review). The standard catalogue for the subject is that published by Abell (1958) (also Abell et al., 1989), which focuses on clusters with more than 50 component galaxies that are fairly close to our galaxy ($z \approx 0.2$).

Optical observations show that there is frequently a Brightest Cluster Galaxy (BCG) or a first-ranked galaxy at the centre of galaxy clusters. These are mostly evolved, elliptical galaxies. Around 20% are surrounded by a low surface brightness envelope; these are also called cD galaxies. These only appear in clusters and groups (Seigar et al., 2006). The red galaxies in the cluster are old and passively evolving, and form a tight sequence in colour-magnitude diagrams (De Lucia et al., 2004). They can be used to locate clusters (e.g. the Red-Sequence Cluster Survey, Gladders and Yee, 2000).

Spectroscopy forms an important part of the optical observations of galaxies in clusters, as it allows the redshifts of the clusters to be measured to high precision ($\Delta z \sim 0.01$). Large-scale surveys aimed at obtaining redshifts for large numbers of galaxies are currently in progress, for example the Sloan Digital Sky Survey (SDSS; York et al., 2000).

Galaxy clusters are complicated, diffuse objects in the optical regime (see Figure 1). It often proves tricky to differentiate between cluster galaxies and foreground galaxies (hence the selection methods used by Abell, 1958). In general, spectroscopic observations of the galaxies are needed to identify their redshifts, so that their line-of-sight difference is known. N-body techniques such as friends-of-friends (see §5.1) can also be applied to select galaxies in clusters (Clewley et al., 2006).

2.2 X-rays

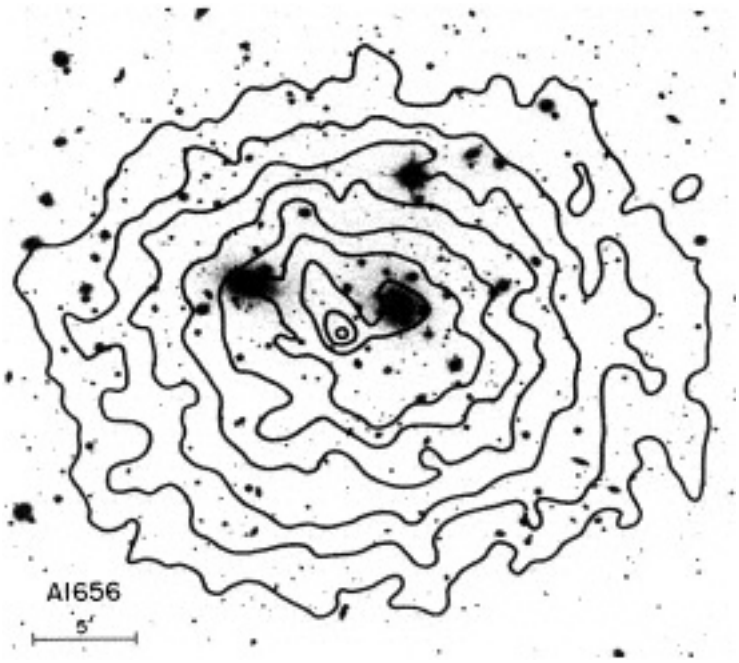

Figure 2: The Coma Cluster (Abell 1656) at 0.15nm (8.0–8.2keV X-rays). From *Einstein* (Jones and Forman, 1999).

Due to the temperature of the gas in the ICM, thermal emission is given off as X-rays mostly via thermal bremsstrahlung, but also through line radiation. The spectral surface brightness at energy E along a particular line of sight l is given by (Birkinshaw, 1999)

$$b(\theta, E) = \frac{1}{4\pi(1+z)^3} \int n_{\rm e}(r)^2 \Lambda(E, T_{\rm e}) dl, \tag{1}$$

where z is the redshift of the cluster, $n_{\rm e}(r)$ is the electron number density and $\Lambda(E, T_{\rm e})$ is the spectral emissivity at X-ray energy E of a gas at temperature $T_{\rm e}$; this function is generally complicated. A related parameter is the cooling function, which gives the total energy emitted from a gas at temperature $T_{\rm e}$.

The intensity of X-rays emitted depends on the square of the electron density, hence X-ray observations only see the cores of the galaxy clusters, rather than the outskirts of the cluster (see Figure 2). The gas in this part of the cluster can be subject to complicating effects including heating and cooling (see e.g. Motl et al., 2005), and the X-ray emission will also be more sensitive to clumps in the gas.

2.3 The Sunyaev-Zel'dovich effect

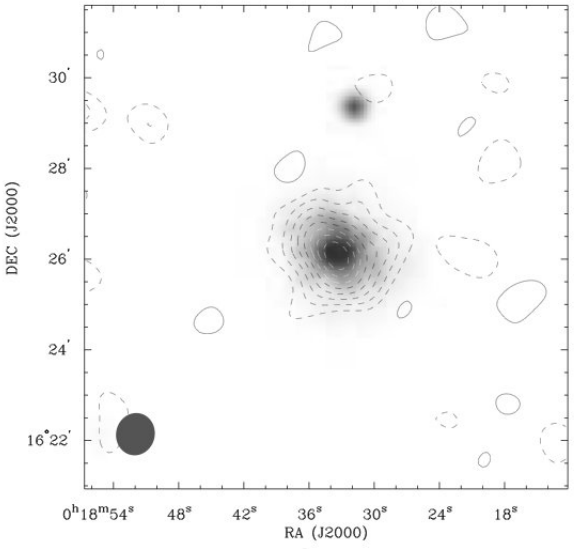

Figure 3: Detection of the SZ effect in CL 0016+16 at 1cm (contours) by the OVRO Millimeter Array superimposed on the X-ray emission from the cluster (grey-scale) by ROSAT (Carlstrom et al., 1996a,b).

The Sunyaev-Zel'dovich effect is due to the inverse Compton scattering of photons from the Cosmic Microwave Background (CMB) when they pass through the hot electron gas in the ICM. It was predicted by Sunyaev and Zeldovich (1970, 1972), based on earlier work by Weymann (1966) and Zeldovich and Sunyaev (1969). It can be parameterized by the Compton $y(\theta)$ parameter, which represents the integrated pressure along the line of sight l, by (Birkinshaw, 1999)

$$y(\theta) = \frac{\sigma_{\rm T} k_{\rm B}}{m_{\rm e} c^2} \int n_{\rm e} T_{\rm e} \ dl, \tag{2}$$

where $\sigma_{\rm T}$ is the Thomson scattering cross-section, $k_{\rm B}$ is Boltzmann's constant, $m_{\rm e}$ is the electron mass, c is the speed of light, $n_{\rm e}$ is again the number density of electrons and $T_{\rm e}$ is the temperature of the electrons. Note that this equation does not include z – the effect is redshift independent. Relativistic corrections to this equation can be found in e.g. Itoh et al. (1998).

This is related to a detectable flux S at frequency ν by

$$S_\nu = \frac{2\nu^2 k_{\rm B} T_{\rm CMB}}{c^2} f(x) \int y(\theta) d\Omega, \tag{3}$$

where $f(x) = x^3 e^x / \left((\tanh(x/2) - 4)(e^x - 1)^2 \right)$ in which $x = h\nu / k_{\rm B} T_{\rm CMB}$ represents the frequency dependence of the effect, and the integral is over the observed section of sky. $T_{\rm CMB}$ is the temperature of the CMB.

The SZ effect has a major advantage with locating clusters in that the magnitude of the effect does not depend on redshift, and as such it should be possible to observe clusters of galaxies out to high redshifts relatively easily. Additionally, the SZ effect only depends on n_e, not n_e^2 as in X-ray, so the outer part of the cluster atmosphere can also be observed (see Figure 3), and less complications will arise from substructure and cooling/heating effects within the cluster (Motl et al., 2005).

Here, we concentrate on the thermal SZ effect. A kinetic SZ effect also exists; see section 5 of the review by Birkinshaw (1999). Depending on the velocity of the cluster relative to the CMB, this may be important.

3 Cosmological probes

As clusters are the largest gravitationally bound structures that we can observe, they provide a good probe of cosmology. The most basic cosmological result that can be obtained from the SZ effect is to confirm that the CMB is indeed primordial – if it interacts with a galaxy cluster at known redshift, then the CMB must have a higher redshift than the cluster (Birkinshaw, 1999).

3.1 Distances and the Hubble parameter

As the SZ effect depends only on $n_{\rm e}$ while the X-ray emission depends on $n_{\rm e}^2$, by substituting for $n_{\rm e}$ in one of the equations the angular diameter distance $d_{\rm A}$ to the cluster can be directly measured (see e.g. Reese et al., 2002). An absolute measurement of the distance to the cluster can then be made using a model of the cluster. This distance measure is independent of all other techniques.

When compared with the redshifts of the clusters, which are normally obtained by spectroscopic measurements, a value for the Hubble constant can be calculated. For an example of such a calculation, see Birkinshaw et al. (1991).

3.2 Number counts

The dependence of the number of clusters with z is given by (Battye and Weller, 2003)

$$\frac{dN}{dz} = \Delta\Omega \frac{dV}{dz d\Omega}(z) \int_{M_{lim}(z)}^{\infty} \frac{dN}{dM}(M,z) dM, \tag{4}$$

where $\Delta\Omega$ is the angular size of the sky being looked at, $\frac{dn}{dM}(M,z)$ is the comoving number density of clusters with mass M and redshift z, and $M_{\rm lim}(z)$ is the minimum mass that is being considered (this is usually the minimum detectable mass size).

$$\frac{dV}{dz d\Omega} = \frac{r(z)^2}{H} = \frac{\left(\int_0^z H^{-1}(z')dz'\right)^2}{H} \tag{5}$$

is the comoving volume in a flat universe, in which $r(z)$ is the coordinate distance and H is the Hubble parameter. An additional parameter, the cluster selection function, can

be added in the integral to represent additional factors such as the scatter of the Mass-Temperature relationship (see Battye and Weller, 2003; Majumdar and Mohr, 2003).

The standard Press-Schechter mass function is (Press and Schechter, 1974; Battye and Weller, 2003)

$$\frac{dn}{dM}(z,M) = -\sqrt{\frac{2}{\pi}}\frac{\rho_{\rm m}(t_0)}{M}\frac{\delta_{\rm c}}{D(z)\sigma_{\rm M}^2}\frac{d\sigma_{\rm M}}{dM}\exp\left(-\frac{\delta_{\rm c}^2}{2D(z)^2\sigma_{\rm M}^2}\right), \tag{6}$$

in which $\delta_{\rm c} = 1.686$, $\rho_{\rm m}(t_0)$ is the present value of the matter density and $\sigma_{\rm M}$ is the current over-density with mass M; this is given by the density power spectrum. $D(z)$ is the growth factor, which is normalized by $D(0) = 1$; the dependence on z can be found from solving the perturbation equation for matter fluctuations (Battye and Weller, 2003). Expressions for this relationship can also be found from N-body simulations (see section 5.1 and e.g. Evrard et al., 2002).

From number counts, constraints on several cosmological parameters can be found, including $\Omega_{\rm M}$ and the equation of state for dark energy.

3.3 Confusion

Confusion can arise between the SZ effect from clusters of galaxies and intrinsic CMB fluctuations; each is a noise source to the other. This presents problems with detecting clusters by the SZ effect; the signal can either be hidden or amplified by the background CMB fluctuations (Lancaster et al., 2004).

Additionally, the SZ effect is expected to dominate over the intrinsic fluctuations in the integrated CMB power spectrum at $l \sim 2500$; the exact scale and shape of the effect depends on the cosmological parameters (see Komatsu and Seljak, 2002). Observations at these angular scales are just starting to become feasible, and it is possible that in recent years the effect has been detected (see Bond et al., 2005; Kuo et al., 2006).

Foreground radio sources, such as Active Galactic Nuclei, can also cause problems with detections of the SZ effect (Lancaster et al., 2004). Observations at multiple frequencies can remove some of these problems, due to the different frequency dependencies of the effects.

4 Analytical models

The two most important parts of a cluster model are the density profile and the mass-temperature relation. The former allows one to calculate $n_{\rm e}$, or equivalently the optical depth τ, while the latter provides T, the temperature of the gas, for arbitrary cluster mass. These then allow the calculation of the size and shape of the SZ effect and X-ray emission.

A series of components are common to most models of the ICM; these are discussed first, before moving on to specific models.

4.1 Model ingredients

Gravitational collapse

The virial radius $r_{\rm vir}$ of the cluster can be calculated by using a spherical infall model (see e.g. Peebles, 1980). This gives

$$r_{\rm vir} = \left(\frac{3M_{\rm vir}}{4\pi\Delta_{\rm c}\rho_{\rm crit}} \right)^{1/3}, \tag{7}$$

where $M_{\rm vir}$ is the virial mass of the cluster. $\rho_{\rm crit}$ is the critical density for the universe to have a closed topology; it is given by

$$\rho_{\rm crit} = \frac{3H^2}{8\pi G}, \tag{8}$$

in which H is the Hubble parameter and G is the gravitational constant. $\Delta_{\rm c}$ is the overdensity of the cluster, defined as

$$\Delta_{\rm c} = \frac{\rho_{\rm cluster}}{\rho_{\rm crit}}. \tag{9}$$

The value for $\Delta_{\rm c}$ depends on the cosmology of the universe; in an Einstein-de Sitter universe, this is exactly $18\pi^2 \approx 178$ (Komatsu and Seljak, 2001). More generally, it can be given to within 5% (between $0.15 < \Omega < 1$) by (Eke et al., 1998; see also Lacey and Cole, 1993)

$$\Delta_{\rm c} \approx 178 \begin{cases} \Omega_{\rm m}^{0.30} & \text{if } \Omega_\Lambda = 0 \\ \Omega_{\rm m}^{0.45} & \text{if } \Omega_{\rm m} + \Omega_\Lambda = 1 \end{cases}. \tag{10}$$

Dark matter density profile

The spherical profiles that are used to describe the distribution of matter within clusters are generally of the form (Suto et al., 1998):

$$\xi(x) = \frac{1}{x^\alpha (1 + x^\delta)^\gamma}, \tag{11}$$

where $x = r/r_{\rm s}$ and α, δ and γ are dimensionless parameters. This profile provides a central core, and inner and outer power-law slopes. $r_{\rm s}$ is a critical radius that describes the turn-over point between the core and the power-law slope, commonly called the core radius. It is defined as $r_{\rm s} = r_{\rm vir}/c$, where c is a concentration parameter. Values for c vary; see Eke et al. (2001) for a compilation. The profile can be truncated at the virial radius $r_{\rm vir}$, which prevents potential divergence in the gas mass (e.g. Birkinshaw, 1999; Battye and Weller, 2003).

Setting $\alpha = 1$, $\delta = 1$, $\gamma = 2$ gives the NFW profile (Navarro et al., 1997; see also §2 of Ostriker et al., 2005). This was found by fitting profiles to dark matter halos (see §5.1), and is now the profile of choice for modeling dark matter halos.

An ellipsoid version of of the profile function would be:

$$\xi(\mathbf{r}) = \frac{1}{\left(\frac{\mathbf{r}^{\mathrm{T}}.\mathbf{M}.\mathbf{r}}{r_{\mathrm{s}}^2}\right)^{\alpha/2}\left(1+\left(\frac{\mathbf{r}^{\mathrm{T}}.\mathbf{M}.\mathbf{r}}{r_{\mathrm{s}}^2}\right)^{\delta/2}\right)^{\gamma}}, \tag{12}$$

where the matrix $\mathbf{M}$ contains the details of the semi-major axes (Birkinshaw, 1999, generalized to a more abstract form).

The profile can be related to the density profile by

$$\frac{\rho(r)}{\rho_{\mathrm{crit}}} = \Delta_{\mathrm{c}}\xi(r). \tag{13}$$

Gas density profile

Setting $\alpha = 0$, $\delta = 2$, $\gamma = \frac{3\beta}{2}$ into (11) gives the well-known β profile

$$\xi\left(x\right) = \frac{1}{\left(1+x^2\right)^{\frac{3\beta}{2}}}, \tag{14}$$

which was originally found by fitting to X-ray observations (Cavaliere and Fusco-Femiano, 1976). It has since been found to be related to hydrostatic equilibrium (see §4.4). It generally gives a good fit to the gas profile in the inner part of clusters.

This can be related to the number density of electrons by

$$n_{\mathrm{e}}(r) = n_{\mathrm{e}0}\xi(r), \tag{15}$$

where $n_{\mathrm{e}0}$ represents the electron density at the core of the cluster.

HydroStatic Equilibrium

The equation of HydroStatic Equilibrium (HSE) describes the balance between the outward pressure of a gas and the gravitational force pulling it inward. It has myriad applications, ranging from the earth's atmosphere, to stellar dynamics, to the gas in clusters of galaxies. Mathematically, it is (Komatsu and Seljak, 2001)

$$\frac{1}{\rho_{\mathrm{gas}}}\frac{dP_{\mathrm{gas}}}{dr} = -G\frac{M(r)}{r^2}, \tag{16}$$

where ρ_{gas} is the gas density, P_{gas} is the gas pressure and $M(r)$ is the mass within radius r from the centre of the cluster.

Virial Theorem

The Virial Theorem states that half of the energy from the gravitational infall of a particle is converted to heat, i.e.

$$\frac{1}{2}E_{\mathrm{P}} = E_{\mathrm{K}}, \tag{17}$$

where E_{P} is the energy released from gravitational infall of the particle and E_{K} is its' resultant kinetic energy. From this, a virial radius r_{vir} can be derived, which will depend on the virial mass in the cluster, M_{vir}, by Equation (7).

Entropy

Voit et al. (2003) state that both the density profile and the temperature of the gas are representations of a more fundamental quantity, the entropy of the gas. The formal definition of the gas entropy is

$$s \equiv \ln K^{3/2} + s_0, \tag{18}$$

where s_0 is a constant, the value of which relies on the mixture of particle masses and

$$K \equiv \frac{P}{\rho^{5/3}} = \frac{k_{\rm B}T}{\mu m_{\rm p}\rho^{2/3}}, \tag{19}$$

where μ is the mean molecular weight and $m_{\rm p}$ is the proton mass. Note that K is frequently named as the entropy of the gas within the literature.

Mass-Temperature Relationship

The simplest model of a cluster would consist of purely gravitational effects, where the gas in the cluster gravitationally collapses with a release of energy into heat by the Virial theorem. Assuming that the cluster is isothermal, this is given by (Birkinshaw, 1999)

$$k_{\rm B}T_{\rm e} \approx \frac{GMm_{\rm p}}{2r_{\rm vir}} \approx 7\left(\frac{M}{3\times10^{14}M_{\odot}}\right)\left(\frac{r_{\rm vir}}{\rm Mpc}\right)^{-1}{\rm keV}. \tag{20}$$

Modifications of this basic equation are covered in the discussions of individual models below.

4.2 A simple model

Battye and Weller (2003) assume a spherical β profile, and introduce an "electron density weighted average temperature" by $\langle T_{\rm e}\rangle_{\rm n} = \int n_{\rm e}T_{\rm e}dl / \int n_{\rm e}dl$. By assuming that clusters are in thermal equilibrium, are virialized (hence the Virial Theorem can be applied) and that virialization only involves gravitational heating, the following equation is deduced for a universe containing dark energy:

$$\langle T_{\rm e}\rangle_n = T_*\left(\Delta_{\rm c}E(z)^2\right)^{1/3}\left(1+(1+3w)\frac{\Omega_{\rm Q}(z)}{\Delta_{\rm c}}\right)(1+z)^{\varepsilon-1}\left(\frac{M_{\rm vir}}{10^{15}h^{-1}M_{\odot}}\right)^{1/\xi}, \tag{21}$$

where T_* is a normalization factor, $E(z) = H/H_0$, $\Omega_{\rm Q}$ is the ratio of dark energy to the critical density of the universe, which is a function of z, and $M_{\odot}$ is the solar mass. The dimensionless parameters $\varepsilon = 1$ and $\xi = 3/2$. The calculated value of T_* is 0.5; however, the authors point out that both observed and simulated clusters point to a T_* between 1.0 and 2.2. They suggest that the value for ξ "could model non-gravitational heat input", and that ε "models deviations from complete virialization". Suggested values are $1.48 \leq \xi \leq 1.98$, with no preference for the value of ε.

4.3 Conservation of energy and a known dark matter profile

Ostriker et al. (2005) start with a known dark matter density profile, from which they deduce the properties of the ICM. They calculate the initial energy of the cluster before adding corrections due to star formation, work done to expand or contract the gas and feedback. They then set the result equal to the final energy of the cluster to determine the state of the gas at the time the currently-detectable radiation was emitted from it.

The initial energy of the gas is calculated by the Virial theorem with a non-negligible surface pressure P_s:

$$E_{\mathrm{P},0} + 2E_{\mathrm{K},0} - 4\pi r_{\mathrm{vir}}^3 P_{\mathrm{s}} = 0. \tag{22}$$

This yields an expression for the initial energy of the gas in terms of the mass, maximum circular velocity, average pressure and critical radius of the gas.

They add allowances for the gas to collapse into stars, hence removing matter from the ICM. They note that the gas that will collapse has a low entropy compared with the rest, and that by removing it the energy per unit mass of the remaining gas will be increased. Factors are also added to account for the expansion or contraction of the gas, and feedback processes due to various effects (e.g. accretion disks of black holes, supernovae, etc.).

They then assume that the gas changes its density profile into a polytropic distribution by an unnamed mechanism, and use the equation of HydroStatic Equilibrium to calculate the final energy.

This process results with three equations that can be solved simultaneously to completely specify the gas. The equations take input values for the virial radius, concentration parameter and maximum circular velocity from a known model of a dark matter halo, as well as values for the adiabatic index, fraction of the mass in stars, feedback efficiency and average pressure.

The above is initially done for an NFW profile; it is subsequently generalized to specify the gas in arbitrary dark matter potentials.

4.4 Hydrostatic Equilibrium

Starting with the equation of HydroStatic Equilibrium, Makino et al. (1998) showed that an almost-equivalent profile to the spherical beta profile could be derived. (For a simpler derivation, see Lancaster et al., 2004.) They assume isothermality, such that the ideal gas law can be used:

$$P = \frac{\rho_{\mathrm{gas}} k_{\mathrm{B}} T}{\mu m_{\mathrm{p}}}. \tag{23}$$

Assuming that the dark matter is distributed according to the NFW profile, they find that the density profile is given by

$$\rho_{\mathrm{gas}}(r) = \rho_{\mathrm{gas},0} e^{-b} \left(1 + \frac{r}{r_{\mathrm{s}}}\right)^{br_s/r}, \tag{24}$$

where $\rho_{\rm gas,0}$ is the central gas density. b is given by

$$b \equiv \frac{4\pi G\mu m_{\rm p}\Delta_{\rm c}(M)\rho_{c0}r_s^2}{k_{\rm B}T} = \frac{3r}{\gamma r_s}\left[\ln\left(1+\frac{r}{r_s}\right) - \frac{r}{r+r_s}\right]^{-1}, \tag{25}$$

in which $\rho_{\rm c0}$ is the core density of the cluster and $\gamma \sim 1$ is a fudge factor that is determined by the efficiency of shock heating in the gas. The remaining parameters are as previously defined.

In Suto et al. (1998), they went on to provide a recipe for creating the density profile in the case of non-isothermality. They do this by assuming a polytropic equation of state for the gas and establishing a second order differential equation for the gas density profile. This equation can then be solved for a given dark matter profile, polytropic index and two parameters that when combined give the amplitude of the halo density. They then suggest that the solved profile is compared to the data and the process restarted with improved input parameters to give a better fit.

Komatsu and Seljak (2001) point out that, while the spherical β profile generally gives a good fit to gas profiles in clusters observed through X-rays (which observe the inner parts of the clusters), it does not describe the outer parts of the clusters well, where the slope of the profile changes. Instead, they suggest that the gas in the outer part of the cluster follows the dark matter distribution.

They adapt the relationships given in Suto et al. (1998) for a non-isothermal gas, and add the requirements that the gas density profile is self-similar, i.e. it obeys

$$\rho_{\rm gas}(r) = \rho_{\rm gas}(0)\xi(r/r_{\rm s}), \tag{26}$$

and that outside the core the gas traces the dark matter distribution. They doe this by having the gas density profile match the dark matter density profile over a region of a factor of 2 above and below the virial radius. This creates a closed solution, with no free parameters.

They use the NFW profile for the dark matter distribution and get the following equation for the gas profile:

$$y_{\rm gas}^{\gamma-1}(x) = 1 - 3\eta^{-1}(x)\frac{\gamma-1}{\gamma}\left(\frac{c}{m(c)}\right)\int_0^x du\frac{m(u)}{u^2}, \tag{27}$$

where the function $m(x)$ is the mass within the dimensionless radius x, c is again the concentration parameter and

$$\eta^{-1}(x) \equiv \frac{G\mu m_{\rm p}M_{\rm vir}}{3r_{\rm vir}k_{\rm B}T_{\rm gas}(x)}. \tag{28}$$

They suggest that $\eta(0)$ and the value of γ are determined by the requirement that the gas traces the dark matter in the specified region, and that the choice does not depend on the value of x that is selected. This can be achieved by numerically fitting the above profile to the other density profiles.

They do not give a Mass–Temperature relationship; rather, they give a Mass–X-ray emission temperature relationship of

$$k_{\rm B}T_{\rm X} = \eta_{\rm X}\frac{G\mu m_p M_{\rm vir}}{3r_{\rm vir}}, \tag{29}$$

where the emission-weighted η_X is given by

$$\begin{aligned}\eta_{\rm X} &= \frac{\int dV \rho^2_{\rm gas}\Lambda(T_{\rm gas})\eta(r)}{\int dV \rho^2_{\rm gas}\Lambda(T_{\rm gas})} \\ &\approx \eta(0)\frac{\int_0^{x_{\rm max}} x^2 dx [y_{\rm gas}(x)]^{(3\gamma+1)/2}}{\int_0^{x_{\rm max}} x^2 dx [y_{\rm gas}(x)]^{(\gamma+3)/2}}.\end{aligned} \tag{30}$$

This can then be related to the actual temperature of the gas by a T_X–T relation.

5 Numerical Simulations

While numerical models are slow to produce results compared to analytical solutions, they are necessary to model the nonlinear evolution of galaxies. Their output can be used as an input to analytical models (see e.g. Section 4.3) and analytical solutions can be found by analyzing their output.

Various approaches to numerical simulations have been utilized for a wide variety of astrophysical problems. There are two main types: N-body and hydrodynamical. Different approaches within each of these types have been taken; here the most commonly used methods are summarized, and examples of relevant simulations are given.

5.1 N-body simulations

N-body simulations use the gravitational force between particles to compute their evolution. They date back to Holmberg (1941), who used an analogue computer system consisting of a series of light-bulbs whose intensity were measured by photocells to simulate two colliding galaxies.

In general, they split the gravitational force into long and short range forces. The short range component is then softened to compensate for the large mass of the particles in the simulation compared to actual objects.

There are various types of N-body simulations, generally named after the types of interactions involved. The main ones include:

- Particle-Particle (PP)
- Particle-Mesh (PM) (see e.g. Hockney and Eastwood, 1981)
- Particle-Particle/Particle-Mesh (P^3M) (Efstathiou and Eastwood, 1981; Efstathiou et al., 1985)
- Tree-Particle-Mesh (TPM) (Xu, 1995; Bode et al., 2000)

N-body simulations are generally used within cosmology for looking at the distributions of clusters (e.g. Retzlaff et al., 1998; Evrard et al., 2002) and their evolution over time. As a result, they can provide expected mass functions and number counts, e.g. Jenkins et al. (2001). Additionally, they can be used to investigations the distribution of dark matter within haloes.

There are a variety of methods for locating clusters within N-body simulations. In the Friends-of-Friends (FOF) method, particle pairs that have a separation of less than a specified fraction of the mean particle separation are linked. Clusters are then found by searching for groups of these linked particles (Davis et al., 1985). This has the advantage that a fixed shape is not assumed, although it can accidentally link separate clusters together by a "chance bridge of particles" (Jenkins et al., 2001).

An alternative is the Spherical Overdensity (SO) method, which involves calculating a local density for each particle based upon its' distance from other particles. Particles with the highest local density are used as the seeds of clusters; a sphere around this particle is then considered, where the edge of the sphere is defined by the position where the local density of the nearest particle to the seed particle falls below a specified value. The centre of mass of the sphere is then calculated; this is then used as the origin of a new sphere, and the process is repeated until the result converges (Lacey and Cole, 1994).

N-body simulations have the major disadvantage that they consume a large amount of CPU hours; the gigaparticle (10^9) simulation run by Evrard et al. (2002) took around 7 months to run on a 512-CPU computer.

For a recent review of the use of N-body simulations in cosmology, see Bagla (2005).

5.2 N-body and hydrodynamical simulations

Hydrodynamical simulations are useful for modeling the intracluster medium. They consist of solving the hydrodynamical equations with various physical effects, such as radiative cooling, adiabatic compression and shock heating (see e.g. Muanwong et al., 2002).

A frequently used type of hydrodynamical simulations is Smooth Particle Hydrodynamics (SPH), which dates back to 1977 (Gingold and Monaghan, 1977; Lucy, 1977). It was originally used to model close binary and non-spherical stars. It works by following the evolution of a finite set of particles, and then smoothing out their properties to form an overall view of the system. The particles can be viewed as a mesh, although it is a very flexible one, or as interpolation points. For a recent review of SPH, see Monaghan (2005).

Early simulations were done by Gull and Northover (1975) and Lea (1976), among others, who performed a one-dimensional hydrodynamical simulation of gas falling into the potential of a cluster. Modern simulations of clusters of galaxies generally consist of two parts - an N-body simulation of the collisionless dark matter, and a hydrodynamic simulation of the intracluster gas. An early example of this is that of Evrard (1988), who combined P^3M N-body simulations with SPH.

An important combined N-body/SPH simulation was that done by Navarro et al. (1995, 1996, 1997), which resulted in the discovery of the well-known NFW profile.

6 Conclusions

In section 2 of this review, we looked at the different types of observations that could be made of galaxy clusters and the ICM, while section 3 discussed the cosmological uses of clusters of galaxies. Of the different observational effects, the Sunyaev-Zel'dovich effect presents the most promising method for selecting galaxy clusters for number counts, which can then be used to constrain cosmological parameters. Combined with X-ray measurements, the SZ effect can also be used to determine the distances to clusters. Optical observations are also of use, mainly in terms of spectroscopic redshift measurements.

Section 4 discussed the components of models of the intracluster medium, and examined three models; those by Battye and Weller (2003), Ostriker et al. (2005) and the combined model of Makino et al. (1998), Suto et al. (1998) and Komatsu and Seljak (2001). These analytical models are important as they determine the density distribution and the mass to temperature relationship in a quick and efficient way, these components in turn determine the magnitudes of the X-ray emission and SZ effect.

Section 5 discussed numerical simulations of both the large-scale structure and the intracluster medium. The former of these are useful as they present artificial skies, which can be used to determine the efficiency that observations will detect clusters (see e.g. Battye and Weller, 2003). The latter provide a means of testing the effect of the various heating and cooling mechanisms within the gas; they also allow the testing of analytical models in a completely specified, 3D situation.

In the near future, large-scale surveys for clusters of galaxies will be carried out, for example the Planck cluster survey, among many others (see e.g. Bartlett, 2006, for a list of upcoming surveys). In the meantime, further work needs to be done to simulate the clusters and the distribution of them in the sky. Additionally, investigation into how well clusters of galaxies can be detected by the different upcoming experiments, and what the expected accuracy on the cosmological parameters will be, also needs to take place.

Acknowledgment

I gratefully acknowledge the support of a PPARC studentship.

References

Abell, G. O. (1958). The Distribution of Rich Clusters of Galaxies. *ApJS*, 3:211.

Abell, G. O., Corwin, Jr., H. G., and Olowin, R. P. (1989). A catalog of rich clusters of galaxies. *ApJS*, 70:1–138.

Bagla, J. S. (2005). Cosmological N-Body simulation: Techniques, Scope and Status. *Current Science*, 88:1088–1100, astro-ph/0411043.

Bartlett, J. G. (2006). SZ Surveys are Coming: What should we do? astro-ph/0606241.

Battye, R. A. and Weller, J. (2003). Constraining cosmological parameters using Sunyaev-Zel'dovich cluster surveys. *Phys. Rev. D*, 68:083506, astro-ph/0305568.

Birkinshaw, M. (1999). The Sunyaev-Zel'dovich Effect. *Phys. Rep.*, 310:97–195, astro-ph/9808050.

Birkinshaw, M., Hughes, J. P., and Arnaud, K. A. (1991). A measurement of the value of the Hubble constant from the X-ray properties and the Sunyaev-Zel'dovich effect of Abell 665. *ApJ*, 379:466.

Biviano, A. (2000). From Messier to Abell: 200 years of science with galaxy clusters. In *Constructing the Universe with clusters of galaxies*. astro-ph/0010409.

Bode, P., Ostriker, J. P., and Xu, G. (2000). The Tree Particle-Mesh N-Body Gravity Solver. *ApJS*, 128:561.

Bond, J. R., Contaldi, C. R., Pen, U.-L., Pogosyan, D., Prunet, S., Ruetalo, M. I., Wadsley, J. W., Zhang, P., Mason, B. S., Myers, S. T., Pearson, T. J., Readhead, A. C. S., Sievers, J. L., and Udomprasert, P. S. (2005). The Sunyaev-Zel'dovich Effect in CMB-calibrated Theories Applied to the Cosmic Background Imager Anisotropy Power at $l > 2000$. *ApJ*, 626:12, astro-ph/0205386.

Carlstrom, J. E., Joy, M., and Grego, L. (1996a). Interferometric Imaging of the Sunyaev-Zeldovich Effect at 30 GHz. *ApJ*, 456:L75.

Carlstrom, J. E., Joy, M., and Grego, L. (1996b). Interferometric Imaging of the Sunyaev-Zeldovich Effect at 30 GHz: Erratum. *ApJ*, 461:L59.

Cavaliere, A. and Fusco-Femiano, R. (1976). X-rays from hot plasma in clusters of galaxies. *A&A*, 49:137–144.

Clewley, L., van Breukelen, C., and Bonfield, D. (2006). Detecting galaxy clusters at $0.1 < z < 2.0$. astro-ph/0612118.

Davis, M., Efstathiou, G., Frenk, C. S., and White, S. D. M. (1985). The evolution of large-scale structure in a universe dominated by cold dark matter. *ApJ*, 292:371–394.

De Lucia, G., Poggianti, B. M., Aragón-Salamanca, A., Clowe, D., Halliday, C., Jablonka, P., Milvang-Jensen, B., Pelló, R., Poirier, S., Rudnick, G., Saglia, R., Simard, L., and White, S. D. M. (2004). The Buildup of the Red Sequence in Galaxy Clusters since z ˜ 0.8. *ApJL*, 610:L77–L80, astro-ph/0406454.

Efstathiou, G., Davis, M., White, S. D. M., and Frenk, C. S. (1985). Numerical techniques for large cosmological N-body simulations. *ApJS*, 57:241.

Efstathiou, G. and Eastwood, J. W. (1981). On the clustering of particles in an expanding universe. *MNRAS*, 194:503.

Eke, V. R., Navarro, J. F., and Frenk, C. S. (1998). The Evolution of X-Ray Clusters in a Low-Density Universe. *ApJ*, 503:569.

Eke, V. R., Navarro, J. F., and Steinmetz, M. (2001). The Power Spectrum Dependence of Dark Matter Halo Concentrations. *ApJ*, 554:144.

Evrard, A. E. (1988). Beyond N-body - 3D cosmological gas dynamics. *MNRAS*, 235:911.

Evrard, A. E., MacFarland, T. J., Couchman, H. M. P., Colberg, J. M., Yoshida, N., White, S. D. M., Jenkins, A., Frenk, C. S., Pearce, F. R., Peacock, J. A., and Thomas, P. A. (2002). Galaxy Clusters in Hubble Volume Simulations: Cosmological Constraints from Sky Survey Populations. *ApJ*, 573:7.

Gingold, R. A. and Monaghan, J. J. (1977). Smoothed particle hydrodynamics - Theory and application to non-spherical stars. *MNRAS*, 181:375.

Gladders, M. D. and Yee, H. K. C. (2000). A New Method For Galaxy Cluster Detection. I. The Algorithm. *AJ*, 120:2148–2162, astro-ph/0004092.

Gull, S. F. and Northover, K. J. E. (1975). Hot gas in clusters of galaxies. *MNRAS*, 173:585–603.

Hockney, R. W. and Eastwood, J. W. (1981). *Computer Simulations Using Particles*. McGraw Hill.

Holmberg, E. (1941). On the Clustering Tendencies among the Nebulae. II. a Study of Encounters Between Laboratory Models of Stellar Systems by a New Integration Procedure. *ApJ*, 94:385.

Itoh, N., Kohyama, Y., and Nozawa, S. (1998). Relativistic Corrections to the Sunyaev-Zeldovich Effect for Clusters of Galaxies. *ApJ*, 502:7.

Jenkins, A., Frenk, C. S., White, S. D. M., Colberg, J. M., Cole, S., Evrard, A. E., Couchman, H. M. P., and Yoshida, N. (2001). The mass function of dark matter haloes. *MNRAS*, 321:372–384, astro-ph/0005260.

Jones, C. and Forman, W. (1999). Einstein observatory images of clusters of galaxies. *ApJ*, 511:65.

Komatsu, E. and Seljak, U. (2001). Universal gas density and temperature profile. *MNRAS*, 327:1353–1366.

Komatsu, E. and Seljak, U. (2002). The Sunyaev-Zel'dovich angular power spectrum as a probe of cosmological parameters. *MNRAS*, 336:1256, astro-ph/0205468.

Kuo, C., Ade, P., Bock, J., Bond, J., Contaldi, C., Daub, M., Goldstein, J., Holzapfel, W., Lange, A., Lueker, M., Newcomb, M., Peterson, J., Reichardt, C., Ruhl, J., Runyan, M., and Staniszweski, Z. (2006). Improved Measurements of the CMB Power Spectrum with ACBAR. *ApJ*, astro-ph/0611198.

Lacey, C. and Cole, S. (1993). Merger rates in hierarchical models of galaxy formation. *MNRAS*, 262:627.

Lacey, C. and Cole, S. (1994). Merger Rates in Hierarchical Models of Galaxy Formation - Part Two - Comparison with N-Body Simulations. *MNRAS*, 271:676–+, astro-ph/9402069.

Lancaster, K., Genova-Santos, R., Falcon, N., Grainge, K., Gutierrez, C., Kneissl, R., Marshall, P., Pooley, G., Rebolo, R., Rubino-Martin, J.-A., Saunders, R. D. E., Waldram, E., and Watson, R. A. (2004). Very Small Array observations of the Sunyaev-Zel'dovich effect in nearby galaxy clusters. *MNRAS*, 359:16–30, astro-ph/0405582.

Lea, S. M. (1976). The dynamics of the intergalactic medium in the vicinity of clusters of galaxies. *ApJ*, 203:569.

Lucy, L. B. (1977). A numerical approach to the testing of the fission hypothesis. *AJ*, 82:1013.

Majumdar, S. and Mohr, J. J. (2003). Importance of Cluster Structural Evolution in Using X-Ray and Sunyaev-Zeldovich Effect Galaxy Cluster Surveys to Study Dark Energy. *ApJ*, 585:603–610, astro-ph/0208002.

Makino, N., Sasaki, S., and Suto, Y. (1998). X-ray gas density profile of clusters of galaxies from the universal dark matter halo. *ApJ*, 497(555), astro-ph/9710344.

Monaghan, J. J. (2005). Smoothed particle hydrodynamics. *Rep. Prog. Phys.*, 68:1703.

Motl, P. M., Hallman, E. J., Burns, J. O., and Norman, M. L. (2005). The Integrated Sunyaev-Zeldovich Effect as a Superior Method for Measuring the Mass of Clusters of Galaxies. *ApJ*, 623:L63.

Muanwong, O., Thomas, P. A., Kay, S. T., and Pearce, F. R. (2002). The effect of cooling and preheating on the X-ray properties of clusters of galaxies. *MNRAS*, 336:527–540, astro-ph/0205137.

Navarro, J. F., Frenk, C. S., and White, S. D. M. (1995). Simulations of X-ray clusters. *MNRAS*, 275:720–740, astro-ph/9408069.

Navarro, J. F., Frenk, C. S., and White, S. D. M. (1996). The Structure of Cold Dark Matter Halos. *ApJ*, 462:563, astro-ph/9508025.

Navarro, J. F., Frenk, C. S., and White, S. D. M. (1997). A Universal Density Profile from Hierarchical Clustering. *ApJ*, 490:493, astro-ph/9611107.

Ostriker, J. P., Bode, P., and Babul, A. (2005). A Simple and Accurate Model for Intra-Cluster Gas. *ApJ*, 634:964, astro-ph/0504334.

Peebles, P. J. E. (1980). *The Large-Scale Structure of the Universe*. Princeton University Press.

Press, W. H. and Schechter, P. (1974). Formation of Galaxies and Clusters of Galaxies by Self-Similar Gravitational Condensation. *ApJ*, 187:425–438.

Reese, E. D., Carlstrom, J. E., Joy, M., Mohr, J. J., Grego, L., and Holzapfel, W. L. (2002). Determining the Cosmic Distance Scale from Interferometric Measurements of the Sunyaev-Zel'dovich Effect. *ApJ*, 581:53–85, astro-ph/0205350.

Retzlaff, J., Borgani, S., Gottloeber, S., Klypin, A., and Mueller, V. (1998). Constraining cosmological models with cluster power spectra. *New Astronomy*, 3:631, astro-ph/9709044.

Seigar, M. S., Graham, A. W., and Jerjen, H. (2006). Intracluster light and the extended stellar envelopes of cD galaxies: An analytical description. astro-ph/0612229.

Sunyaev, R. A. and Zeldovich, Y. B. (1970). Small-Scale Fluctuations of Relic Radiation. *Astrophysics and Space Science*, 7:3.

Sunyaev, R. A. and Zeldovich, Y. B. (1972). The Observation of Relic Radiation as a Test of the Nature of X-Ray Radiation from the Clusters of Galaxies. *Comments on Astrophysics and Space Physics*, 4:173.

Suto, Y., Sasaki, S., and Makino, N. (1998). Gas density and X-Ray surface brightness profiles of clusters of galaxies from dark matter halo potentials: beyond the isothermal β model. *ApJ*, 509:544.

Voit, G. M. (2004). Tracing cosmic evolution with clusters of galaxies. astro-ph/0410173.

Voit, G. M., Balogh, M. L., Bower, R. G., Lacey, C. G., and Bryan, G. L. (2003). On the Origin of Intracluster Entropy. *ApJ*, 593:272.

Weymann, R. (1966). The Energy Spectrum of Radiation in the Expanding Universe. *ApJ*, 145:560.

Xu, G. (1995). A New Parallel N-Body Gravity Solver: TPM. *ApJS*, 98:355.

York, D. G., Adelman, J., Anderson, John E., J., Anderson, S. F., Annis, J., Bahcall, N. A., Bakken, J. A., Barkhouser, R., Bastian, S., Berman, E., Boroski, W. N., Bracker, S., Briegel, C., Briggs, J. W., Brinkmann, J., Brunner, R., Burles, S., Carey, L., Carr, M. A., Castander, F. J., Chen, B., Colestock, P. L., Connolly, A. J., Crocker, J. H., Csabai, I., Czarapata, P. C., Davis, J. E., Doi, M., Dombeck, T., Eisenstein, D., Ellman, N., Elms, B. R., Evans, M. L., Fan, X., Federwitz, G. R., Fiscelli, L., Friedman, S., Frieman, J. A., Fukugita, M., Gillespie, B., Gunn, J. E., Gurbani, V. K., de Haas, E., Haldeman, M., Harris, F. H., Hayes, J., Heckman, T. M., Hennessy, G. S., Hindsley, R. B., Holm, S., Holmgren, D. J., Huang, C.-h., Hull, C., Husby, D., Ichikawa, S.-I., Ichikawa, T., Ivezić, Ž., Kent, S., Kim, R. S. J., Kinney, E., Klaene, M., Kleinman, A. N., Kleinman, S., Knapp, G. R., Korienek, J., Kron, R. G., Kunszt, P. Z., Lamb, D. Q., Lee, B., Leger, R. F., Limmongkol, S., Lindenmeyer, C., Long, D. C., Loomis, C., Loveday, J., Lucinio, R., Lupton, R. H., MacKinnon, B., Mannery, E. J., Mantsch, P. M., Margon, B., McGehee, P., McKay, T. A., Meiksin, A., Merelli, A., Monet, D. G., Munn, J. A., Narayanan, V. K., Nash, T., Neilsen, E., Neswold, R., Newberg, H. J., Nichol, R. C., Nicinski, T., Nonino, M., Okada, N., Okamura, S., Ostriker, J. P., Owen, R., Pauls, A. G., Peoples, J., Peterson, R. L., Petravick, D., Pier, J. R., Pope, A., Pordes, R., Prosapio, A., Rechenmacher, R., Quinn, T. R., Richards, G. T., Richmond, M. W., Rivetta, C. H., Rockosi, C. M., Ruthmansdorfer, K., Sandford, D., Schlegel, D. J., Schneider, D. P., Sekiguchi, M., Sergey, G., Shimasaku, K., Siegmund, W. A., Smee, S., Smith, J. A., Snedden, S., Stone, R., Stoughton, C., Strauss, M. A., Stubbs, C., SubbaRao, M., Szalay, A. S., Szapudi, I., Szokoly, G. P., Thakar, A. R., Tremonti, C., Tucker, D. L., Uomoto, A., Vanden Berk, D., Vogeley, M. S., Waddell, P., Wang, S.-i., Watanabe, M., Weinberg, D. H., Yanny, B., and Yasuda, N. (2000). The Sloan Digital Sky Survey: Technical Summary. *AJ*, 120:1579.

Zeldovich, Y. B. and Sunyaev, R. A. (1969). The interaction of matter and radiation in a hot-model universe. *Astrophysics and Space Science*, 4(3):301.